

Article

# MAS-Based Decentralized Coordinated Control Strategy in a Micro-Grid with Multiple Microsources

Shiyun Xu <sup>1</sup>, Huadong Sun <sup>1</sup>, Zhanqiang Zhang <sup>2,\*</sup> , Qiang Guo <sup>1</sup>, Bin Zhao <sup>1</sup>, Jingtian Bi <sup>1</sup> and Bo Zhang <sup>2,\*</sup>

<sup>1</sup> China Electric Power Research Institute, Beijing 100192, China; xushiyun@epri.sgcc.com.cn (S.X.); sunhd@epri.sgcc.com.cn (H.S.); guoqiang@epri.sgcc.com.cn (Q.G.); zhaobing@epri.sgcc.com.cn (B.Z.); bijingtian@epri.sgcc.com.cn (J.B.)

<sup>2</sup> Institute of Electrical Engineering, Yanshan University, Qinhuangdao 066044, China

\* Correspondence: zhanqiangzhangysu@163.com (Z.Z.); zb516869613@163.com (B.Z.); Tel.: +86-15690326186 (Z.Z.); +86-18332532506 (B.Z.)

Received: 26 February 2020; Accepted: 22 April 2020; Published: 30 April 2020



**Abstract:** In this paper, a decentralized coordinated control method based on multi-agent system is proposed to improve the voltage stability of micro-grid. In lower-level agents, the decentralized control is designed as double-loop controllers for the inverter of each distributed energy resource, including an outer-loop power controller based on droop control and an inner-loop voltage/current controller based on fractional order proportion-integral-derivative (PID). In upper-level agents, the distributed coordinated control is designed to make voltage consensus and proportional power sharing of all distributed energy resources. Since each distributed coordinated control only requires its own and neighboring information, the communication bandwidth can be saved. The simulation results have verified the effectiveness in terms of power sharing, voltage stability, and suppressing circulation current.

**Keywords:** multi-agent system; micro-grid; decentralized control; coordinated control

## 1. Introduction

With the increasing concern of the high carbon emission and the limited fossil fuel reserves, the renewable energy generation has become a popular research topic. In recent times, the distributed generation (DG) technologies to develop the clean renewable energies have been widely used in power supply system [1,2]. Currently, the major types of DGs include photovoltaic (PV), wind turbine (WT), micro turbines (MT), fuel cell (FC), etc. However, as the DG technologies are used in micro-grid (MG) system, DGs present the quasi-load characteristics. Standard IEEE 1547 has set the rules regarding DG grid connection which requires withdrawal operation of each micro generation when any fault occurs in MG. This greatly reduces the utilization efficiency of distributed energy resource. For the sake of coordinating the conflict between the grid and DGs, fully exploiting the potential of distributed energy resource and promoting larger scale of application of DG technology, the notion of MG has been advocated [3,4].

Two operation modes can be applied in MG including the grid-connected mode and islanded mode [5,6]. In grid-connected mode, the MG can absorb the power from main grid or inject power into main grid, and the voltage and the frequency are determined by the main grid. When the fault occurs in main grid, the MG has to disconnect from the utility grid, and meanwhile it needs to maintain the stability of voltage and frequency and provide the uninterruptible power supply for critical loads. Therefore, the efficient strategies must be proposed to control the DGs.

A majority of DGs are connected to MG through the inverters, so the control strategies of inverters are of great importance. Currently, the research on the inverter control has received extensive attention. The control strategies of inverter can be mainly divided into centralized control and decentralized control [7]. In the centralized control, all controllers are unified managed by a central controller. If the central controller fails, the entire MG system will lose its stability. Also, it needs a reliable communication network to support the information interaction. The decentralized control means that each DG only requires knowing its own information to complete the inverter control. Each DG is controlled by the local controller without communication links. Taking a typical decentralized control-droop control as an example, this method can share the total power of load demand directly according to the droop coefficients, and thus determine the voltage and frequency of DG. It does not need a central controller, and gives full play to the “plug and play” advantage of distributed power supply, i.e., DGs can be directly added into MG to work normally. However, as the number of DG in MG increases and meanwhile the necessary information interaction between DGs is unavailable, it is difficult for this control mode to coordinate DGs’ output, which in turn makes the requirements of grid operation unsatisfied. In order to weigh the two methods, the decentralized coordinated control based on consensus in multi-agent system (MAS) is presented in this paper. The main objectives are improving the power sharing accuracy and voltage regulation stability.

So far, some related designs have been proposed. To improve the power sharing, a novel decentralized control method was used to accomplish the suitable load sharing in [8], and a novel active power sharing method with event-triggered mechanism was proposed in [9]. However, these methods do not consider the voltage stability. Therefore, it is likely that the deviation between DGs’ output voltages will cause the existence of circulation current, which will affect the normal operation of MG. Voltage regulation strategy by using consensus-based secondary control is designed to achieve the consistency of DG output voltage and avoid the circulation current in [10–14]. However, these studies only consider improving droop control or adding secondary control, but not consider the tracking performance of voltage/current double-loop control. If the deviation between the input voltage of voltage loop and the output voltage of current loop is large, there will still be the risk of circulation current. To solve these problems, we have designed a coordinated controller based on the consensus algorithm to adjust the voltage and power simultaneously. In addition, we have also designed a FOPID controller to improve the tracking ability of voltage/current double-loop control. With the consensus algorithm, the problem of circulation current can be also suppressed by the voltage regulation of DGs.

In summary, the significant features of the proposed control method are given as follows.

1. A two-level hierarchical control strategy based on MAS is proposed. Each lower-level agent is to implement the decentralized control for the voltage tracking of local DG. The upper-level agents are to implement the coordinated control for voltage consensus and proportional power sharing of all neighboring DGs.
2. The distributed control in the lower-level agent is designed as a double-loop controller. The power controller of outer-loop is developed based on the droop control to achieve the function of wireless communication between the paralleled inverters. To improve the stability of voltage tracking, the fractional order PID (FOPID) instead of the conventional PID is used in voltage controller and current controller of inner-loop.
3. The DGs’ cooperation in coordinated control based on consensus algorithm does not require the global information of MG. Each upper-level agent only exchanges the information with its neighbors via a sparse communication network. Thus, it is more flexible and reliable to achieve the voltage regulation and proportional power sharing.

The remainder of paper is organized as follows. The structure of MG based on MAS is established in Section 2. In Section 3, the decentralized control method of DG is presented. In Section 4, the coordinated control with the consensus algorithm is discussed. Section 5 gives the analysis of circulating current. The simulation studies are given in Section 6. Section 7 summarizes this paper.

## 2. Hierarchical Control Strategy Based on MAS

Multi-agent technology is a branch of artificial intelligence technology [15,16]. Distributed performance of the agent can be adapted to the complicated environment of MG system effectively. The multi-agent hierarchical control technology that can guarantee the stability of the MG system operation is presented in [17,18]. The constructed MAS-based MG is shown in Figure 1.

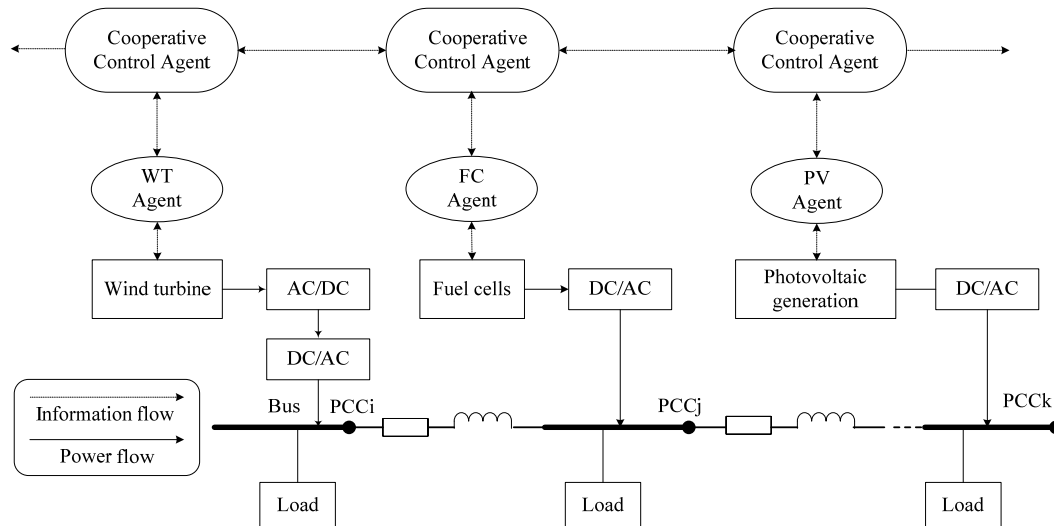


Figure 1. Structure of micro-grid (MG) based on multi-agent system (MAS).

In this network, the consensus of multi-agent is to reach the agreement on specific regions considering their own state information. Consensus algorithm is a specified interaction criterion that the information exchanges between an agent and neighboring agents via a communication network [19–21]. The theoretical framework of consensus algorithm focuses the research on robustness and delay of system with the directed information flow and the change of topology structure [22].

The architectures of different hierarchical agents and the interaction among them are designed in this paper. The lower-level agent consists of a reactive layer and a deliberative layer. The reactive layer is defined as “perception and action,” which has priority to respond quickly to the emergencies of environment. The deliberative layer is defined as “belief, desire, and intention,” which has a high intelligence in controlling or planning the behaviors of agent so as to achieve its intention. The upper-level cooperative control agent is designed as a deliberative agent. The agent is mainly responsible for the secondary control to implement distributed voltage regulation and equal current sharing. In addition, the outputs of the regulators are sent to the lower-level agent through action module, which acts as the control inputs of droop control. The architecture of hierarchical control strategy based on MAS is shown in Figure 2.

## 3. Distributed Coordinated Control Strategy for DG

The MG system is connected to the main grid through point of common coupling (PCC). When a fault occurs in main grid, the MG operates in the islanded mode to ensure the voltage stability and the power sharing accuracy. In this section, the decentralized controller is designed in the lower-level agents. As shown in Figure 3, the outer-loop power controller adopts the droop control [23,24], and the inner-loop voltage/current controller adopts the FOPID controller. In Figure 3,  $L_f$ ,  $R_f$ , and  $C_f$  are the inductance, resistance, and capacitance of filter, respectively;  $L$  and  $R$  are the inductance and resistance of feeder, respectively;  $v_o$  is the actual filter voltage;  $i_l$  and  $i_o$  are the actual filter current and feeder current, respectively;  $P$  and  $Q$  are the actual active power and reactive power, respectively;  $P_n$  and  $Q_n$  are the corresponding nominal powers;  $v_{od}^*$ ,  $v_{oq}^*$  represent the d-axis and q-axis voltage references of the voltage-loop FOPID controller that are outputted from the power controller, respectively; and

$i_{ld}^*, i_{lq}^*$  represent the d-axis and q-axis current references of the current-loop FOPID controller that are outputted from the FOPID voltage controller. The d-axis and q-axis references are actually the control references of FOPID controller which can be used to obtain the input errors for the FOPID controller. Through the FOPID controller, the final PWM signal is obtained for inverter.

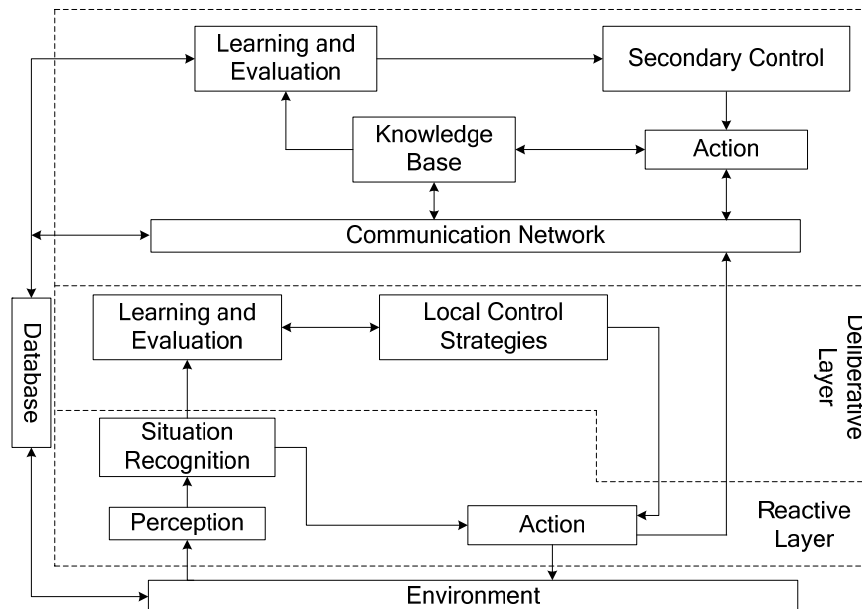


Figure 2. Architecture of hierarchical control strategy based on MAS.

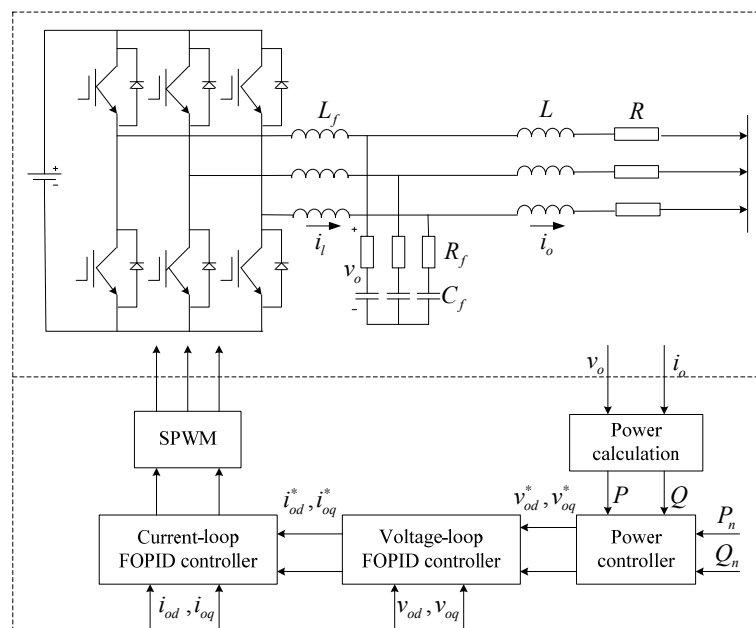


Figure 3. Block diagram of distributed generation (DG) inverter control.

### 3.1. Design of Outer-Loop Power Controller

By using the active power-frequency (P-f) and reactive power-voltage amplitude (Q-U) droop controls, the outer-loop power controller is designed in Figure 4. The instantaneous active power and reactive power can be expressed as:

$$\tilde{p} = v_{od}i_{od} + v_{oq}i_{oq} \tag{1}$$

$$\tilde{q} = v_{od}i_{oq} - v_{oq}i_{od} \tag{2}$$

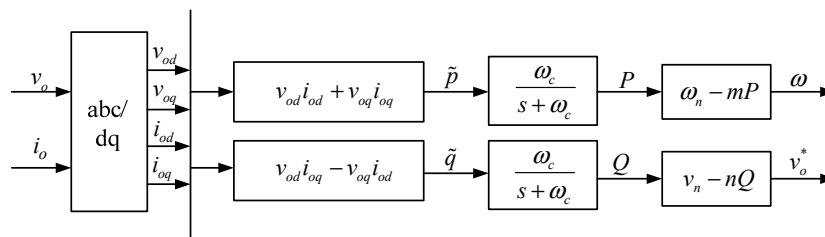


Figure 4. Block diagram of power controller.

Since the direct application of instantaneous power may impact the DG's power quality when MG suffers disturbance, the average power method [25–27] is adopted in this paper. Consider the low-voltage MG dominated by inductive feeder. The P-f and Q-U droop controls are presented as:

$$f = f_n - m(P - P_n) \quad (3)$$

$$v = v_n - n(Q - Q_n) \quad (4)$$

where  $m$  and  $n$  are the P-f droop coefficient and Q-U droop coefficient, respectively, which are usually chosen based on the active and reactive power rating of the DG;  $f_n$  and  $v_n$  are the frequency reference and voltage amplitude reference generated by the output  $y(t)$  in Section 4.2, respectively; and  $P_n$  and  $Q_n$  are the nominal active power and nominal reactive power, respectively. With the output of P-f and Q-U droop controls, the voltage reference  $v_o^*$  as the input of voltage-loop FOPID controller can be obtained.

### 3.2. Design of Inner-Loop Voltage/Current FOPID Controller

FOPID controller proposed by Podlubny in 1999 is the expansion of the conventional PID controller based on fractional calculus [28,29]. It can obtain a better performance than the conventional PID controller. FOPID controller has three parameters: the proportional coefficient  $K_P$ , the integral coefficient  $K_I$ , and the differential coefficient  $K_D$ . They affect the speed of control, the accuracy of control, and the stability of control system, respectively. There are also two adjustable parameters: the integral order  $\lambda$  and the differential order  $\mu$ .

The voltage-loop FOPID controllers (including d-axis and q-axis) are designed as:

$$u(t) = K_{PV}e(t) + K_{IV}D^{-\lambda}e(t) + K_{DV}D^{\mu}e(t) \quad (5)$$

where  $e(t) = v_o - v_o^*$ ;  $u(t) = i_1^*$ , and  $i_1^*$  is the current reference of current-loop FOPID controller;  $K_{PV}$ ,  $K_{IV}$ , and  $K_{DV}$  represent the proportional coefficient, integral coefficient, and differential coefficient in voltage-loop FOPID controller, respectively; and  $\lambda, \mu \in [0, 2]$ .

The current-loop FOPID controllers (including d-axis and q-axis) are designed as:

$$u(t) = K_{PC}e(t) + K_{IC}D^{-\alpha}e(t) + K_{DC}D^{\beta}e(t) \quad (6)$$

where  $e(t) = i_1 - i_1^*$ ;  $u(t) = v^*$ , and  $v^*$  is the final voltage signal for SPWM;  $K_{PC}$ ,  $K_{IC}$ , and  $K_{DC}$  represent the proportional coefficient, integral coefficient, and differential coefficient in current-loop FOPID controller, respectively; and  $\alpha, \beta \in [0, 2]$ .

The relationship between the FOPID control and conventional PID control is shown in Figure 5, where the shaded range represents the control margin of FOPID controller. The FOPID controller generalizes the conventional PID control and expands it from point to plane. This expansion could provide much more flexibility in inner-loop voltage/current controller design to achieve the stable voltage tracking control. Hence, the conventional PID control can be viewed as a special case of the FOPID control. By setting reasonable parameters, FOPID can improve the voltage tracking control effect. The block diagram of inner-loop voltage/current FOPID controller is shown in Figure 6.

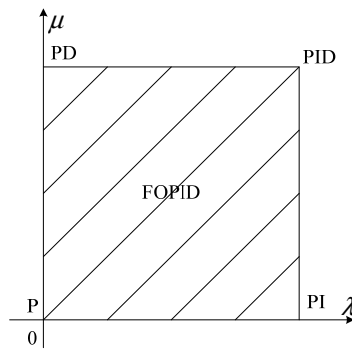


Figure 5. Relationship between fractional order PID (FOPID) control and conventional PID control.

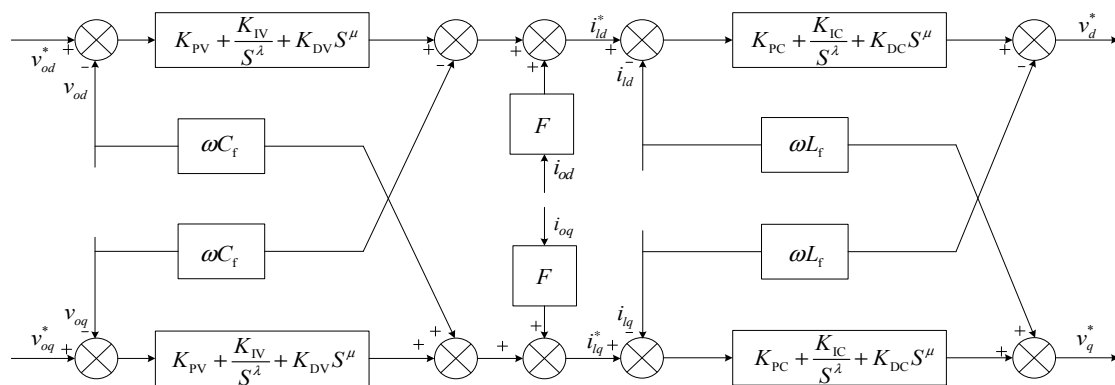


Figure 6. Block diagram of inner-loop voltage/current FOPID controller.

It can be seen from Figure 6 that the inner-loop is composed of voltage-loop and current-loop. The input of voltage-loop FOPID controller is the error between voltage reference  $v_o^*$  from power controller and actual voltage  $v_o$  from DG system. After decoupling (removing the influences of capacitance voltage and inductance current), the output of voltage-loop FOPID controller is the current reference  $i_d^*$  which is also the input of current-loop FOPID controller. After decoupling, the output of current-loop FOPID controller is a triggered voltage, which is used to generate a SPWM signal to control the output of DG inverter.

$$\chi_d = (K_{PV} + K_{IV}S^{-\lambda} + K_{DV}S^{\mu})(v_{od}^* - v_{od}) \tag{7}$$

$$\chi_q = (K_{PV} + K_{IV}S^{-\lambda} + K_{DV}S^{\mu})(v_{oq}^* - v_{oq}) \tag{8}$$

$$\psi_{od} = (K_{PC} + K_{IC}S^{-\alpha} + K_{DC}S^{\beta})(i_{id}^* - i_{id}) \tag{9}$$

$$\psi_{oq} = (K_{PC} + K_{IC}S^{-\alpha} + K_{DC}S^{\beta})(i_{iq}^* - i_{iq}) \tag{10}$$

The assist terms in voltage-loop FOPID controller are given as follow:

$$ASS_d = Fi_{od} - \omega C_f v_{oq} \tag{11}$$

$$ASS_q = Fi_{oq} + \omega C_f v_{od} \tag{12}$$

where  $ASS_d$  and  $ASS_q$  are the d-axis and q-axis regulation terms, respectively; and  $F$  is the feed-forward parameter in the voltage-loop.

The assist terms refer to the regulation terms in current-loop, which are affected by the current, voltage, and filter capacitance. When the output of voltage-loop subtracts these adjusting items, the current reference of current-loop is obtained for the subsequent FOPID controller.

**Remark 1.** The purpose is to decouple the active and reactive power regulations, i.e., when one of them is adjusted, the other will not be affected. Moreover, in the current-loop, these inputs are all subtracted items, so they all belong to the same auxiliary variable.

The outputs of the voltage-loop FOPID controller are presented as:

$$\dot{i}_{1d}^* = \chi_d + ASS_d \quad (13)$$

$$\dot{i}_{1q}^* = \chi_q + ASS_q \quad (14)$$

The outputs of the current-loop FOPID controller are presented as:

$$v_d^* = \psi_d - \omega L_f i_{1q} \quad (15)$$

$$v_q^* = \psi_q + \omega L_f i_{1d} \quad (16)$$

Since the FOPID controller appends fractional order derivative and fractional order integral in comparison with conventional PID controller, it is much difficult to design the FOPID controller. With the simplicity, low computational cost, and good performance, the Particle Swarm Optimization (PSO) as a promising optimization algorithm can be used here to design the parameters [30–33].

As shown in Figure 7, the procedures of the PSO algorithm are described as follows:

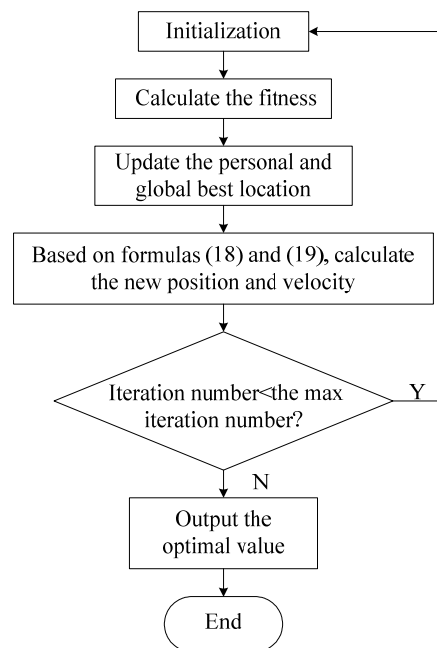


**Figure 7.** Flowchart of Particle Swarm Optimization (PSO) algorithm.

Step 1: Initialization parameters. Determine the number of particles, the dimensions of search space, the value range of parameters, the maximum number of iterations, the learning factor, and the inertia weight coefficients.

Step 2: Initialization particles.

Step 3: Determine the objective function. The integral performance of absolute error is considered as the objective function. In order to get a good dynamic performance and to avoid large control inputs, the fitness function is designed as:

$$F(t) = 1 / \left( \int_0^{\infty} (\rho_1 |e_p(t)| + \rho_2 u_p(t)) dt + \rho_3 t_u \right) \quad (17)$$

where  $e_p(t)$  is the absolute error;  $u_p(t)$  is the control output;  $t_u$  is the rise time, and  $\rho_1, \rho_2, \rho_3$  are the weight coefficients.

Step 4: Calculate the fitness value of each particle. According to the fitness function  $F(t)$ , up the date personal and global best value.

Step 5: The velocity and position update equations are given as:

$$V_i(t+1) = c_0 V_i(t) + c_1 \phi_1 [P_i(t) - X_i(t)] + c_2 \phi_2 [G_i(t) - X_i(t)] \quad (18)$$

$$X_i(t+1) = X_i(t) + V_i(t) \quad (19)$$

where  $c_0$  is the inertia weight;  $c_1$  and  $c_2$  are the positive constant learning rates;  $\phi_1$  and  $\phi_2$  are the random numbers between 0 and 1;  $G_i(t)$  is the global optimal solution in PSO algorithm.

Step 6: Use MATLAB simulation to obtain the optimal value of each parameter.

#### 4. Design of Coordinated Controller based on Consensus Algorithm

The coordinated control is a regulator synchronization problem for DG regulator. In this section, the multi-agent consensus algorithm [33–37] is used to coordinate the output voltage of DGs. Each DG can be seen as an agent, which only requires its own information and the neighbors' information. The control signals are calculated based on the error between local information and one of the neighbors' information. Graph theory plays a crucial role in the analysis of consensus problems.

##### 4.1. Graph Theory

The communication network of a multi-agent cooperative system can be modelled by an undirected graph  $G = (V, \varepsilon, A)$ , where  $V = \{v_1, \dots, v_N\}$  is the set of vertices,  $\varepsilon \subset V \times V$  is the edges, and  $A = [a_{ij}] \in \mathbb{R}^{N \times N}$  is the weighted adjacency matrix. DGs are recognized as the nodes of communication graph of MG. An edge from node  $j$  to node  $i$  is denoted by  $(v_j, v_i)$ , which means the information from node  $j$  can be acquired by node  $i$ .  $a_{ij}$  is the weight of edge  $(v_j, v_i)$  and  $a_{ij} > 0$  if  $(v_j, v_i) \in \varepsilon$ , otherwise  $a_{ij} = 0$ . There are no repeated edges, i.e.,  $a_{ii} = 0, \forall i \in N$ . The degree matrix of  $G$  is  $D_G = \text{diag}\{d_1, \dots, d_N\} \in \mathbb{R}^{N \times N}$ , where  $d_i = \sum_{j \in N_i} a_{ij}$ , and then the Laplacian matrix is defined as  $L = D_G - A$ .

For a given matrix  $M$ ,  $\sigma_{\max}(M)$  denotes the maximal singular values, and  $\sigma_{>0\min}(M)$  denotes the minimal nonzero singular value.

**Definition 1.** Let  $M = [m_{ij}] \in \mathbb{R}^{m \times n}$ ,  $N = [n_{ij}] \in \mathbb{R}^{p \times q}$ . Then the following block matrix is called the Kronecker product of  $M$  and  $N$ , written as:

$$M \otimes N = \begin{bmatrix} m_{11} \cdot N & \cdots & m_{1n} \cdot N \\ \vdots & \ddots & \vdots \\ m_{m1} \cdot N & \cdots & m_{mn} \cdot N \end{bmatrix} \in \mathbb{L}^{mp \times nq}$$

##### 4.2. Design of Coordinated Controller

Without loss of generality, we assume that the  $i$ th DG is connected with other DGs through DG line impedances. In this part, the single-line diagram of the MG test system is shown in Figure 8.

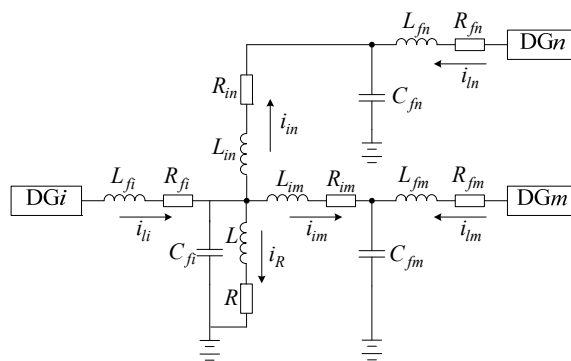


Figure 8. Structure of equivalent circuit of DGs in a MG.

Applying Kirchoff’s voltage law and Kirchoff’s current law to the electrical scheme of Figure 8 can get the following dynamic equations:

$$\begin{cases} \frac{di_{li}}{dt} = -\frac{R_{fi}}{L_{fi}}i_{li} - \frac{1}{L_{fi}}v_i + \frac{1}{L_{fi}}v_{oi} \\ \frac{dv_i}{dt} = \frac{1}{C_{fi}}i_{li} - \frac{R}{L}i_R - \frac{1}{C_{fi}}i_{im} - \frac{1}{C_{fi}}i_{in} \\ \frac{di_R}{dt} = -\frac{R}{L}i_R + \frac{1}{L}v_i \\ \frac{di_{im}}{dt} = -\frac{R_{im}}{L_{im}}i_{im} - \frac{1}{L_{im}}v_m + \frac{1}{L_{im}}v_i \\ \frac{di_{lm}}{dt} = -\frac{R_{fm}}{L_{fm}}i_{lm} - \frac{1}{L_{fm}}v_m + \frac{1}{L_{fm}}v_{om} \\ \frac{dv_m}{dt} = \frac{1}{C_{fm}}i_{lm} + \frac{1}{C_{fm}}i_{im} \\ \frac{di_{in}}{dt} = -\frac{R_{in}}{L_{in}}i_{in} - \frac{1}{L_{in}}v_n + \frac{1}{L_{in}}v_i \\ \frac{di_{ln}}{dt} = -\frac{R_{fn}}{L_{fn}}i_{ln} - \frac{1}{L_{fn}}v_n + \frac{1}{L_{fn}}v_{on} \\ \frac{dv_n}{dt} = \frac{1}{C_{fn}}i_{ln} + \frac{1}{C_{fn}}i_{in} \end{cases} \quad (20)$$

The system model can be described as follow:

$$\begin{cases} \dot{\mathbf{x}}(t) = \mathbf{Ax}(t) + \mathbf{Bu}(t) \\ \mathbf{y}(t) = \mathbf{Cx}(t) \end{cases} \quad (21)$$

where  $\mathbf{x}(t) = [i_{li} \ v_i \ i_R \ i_{im} \ i_{lm} \ v_m \ i_{in} \ i_{ln} \ v_n]^T$  is the state vector,  $\mathbf{u}(t) = [v_{oi} \ v_{om} \ v_{on}]^T$  is the control input, and  $\mathbf{y}(t) = [v_i \ v_m \ v_n]^T$  is the control output. All matrices in (21) are given as follows:

$$\mathbf{A} = \begin{bmatrix} -\frac{R_{fi}}{L_{fi}} & -\frac{1}{L_{fi}} & 0 & 0 & 0 & 0 & 0 & 0 & 0 \\ \frac{1}{C_{fi}} & 0 & -\frac{1}{C_{fi}} & -\frac{1}{C_{fi}} & 0 & 0 & -\frac{1}{C_{fi}} & 0 & 0 \\ 0 & \frac{1}{L} & \frac{R}{L} & 0 & 0 & 0 & 0 & 0 & 0 \\ 0 & \frac{1}{L_{im}} & 0 & -\frac{R_{im}}{L_{im}} & 0 & -\frac{1}{L_{im}} & 0 & 0 & 0 \\ 0 & 0 & 0 & 0 & -\frac{R_{fm}}{L_{fm}} & -\frac{1}{L_{fm}} & 0 & 0 & 0 \\ 0 & 0 & 0 & \frac{1}{C_{fm}} & \frac{1}{C_{fm}} & 0 & 0 & 0 & 0 \\ 0 & \frac{1}{L_{in}} & 0 & 0 & 0 & 0 & -\frac{R_{in}}{L_{in}} & 0 & -\frac{1}{L_{in}} \\ 0 & 0 & 0 & 0 & 0 & 0 & 0 & -\frac{R_{fn}}{L_{fn}} & -\frac{1}{L_{fn}} \\ 0 & 0 & 0 & 0 & 0 & 0 & \frac{1}{C_{fn}} & \frac{1}{C_{fn}} & 0 \end{bmatrix}$$

$$\mathbf{B} = \begin{bmatrix} \frac{1}{L_{fi}} & 0 & 0 \\ 0 & 0 & 0 \\ 0 & 0 & 0 \\ 0 & 0 & 0 \\ 0 & \frac{1}{L_{fm}} & 0 \\ 0 & 0 & 0 \\ 0 & 0 & 0 \\ 0 & 0 & \frac{1}{L_{fn}} \\ 0 & 0 & 0 \end{bmatrix}$$

$$, \mathbf{C} = \begin{bmatrix} 0 & 1 & 0 & 0 & 0 & 0 & 0 & 0 & 0 \\ 0 & 0 & 0 & 0 & 0 & 1 & 0 & 0 & 0 \\ 0 & 0 & 0 & 0 & 0 & 0 & 0 & 0 & 1 \end{bmatrix}$$

In the cooperative consensus problem, it is desired for all DGs to achieve the same state. The neighboring error of the  $i$ th DG is defined as:

$$\hat{e}_i = \sum_{j=m,n} a_{ij}(\hat{v}_i - \hat{v}_j) \tag{22}$$

where  $\hat{e}_i$  and  $\hat{v}_i$  represent the per unit value of corresponding parameters.

The overall neighboring error is  $\hat{e} = (\mathbf{L} \otimes \mathbf{I}_N) \hat{\mathbf{y}}$ , where  $\hat{e} = [\hat{e}_i \ \hat{e}_m \ \hat{e}_n]^T$  and  $\hat{\mathbf{y}} = [\hat{v}_i \ \hat{v}_m \ \hat{v}_n]^T$ . Let  $\hat{\mathbf{u}}(t) = -c\mathbf{H}\hat{e}$ , where  $\hat{\mathbf{u}}(t)$  is the per unit value, and  $\mathbf{H}$  is the feedback gain matrix. The corresponding global form is written as:

$$\mathbf{u}(t) = -c(\mathbf{L} \otimes \mathbf{H}) \hat{\mathbf{y}} \tag{23}$$

So the overall closed-loop system dynamics are described by:

$$\dot{\hat{\mathbf{x}}}(t) = (\mathbf{I}_N \otimes \mathbf{A} - c\mathbf{L} \otimes \mathbf{BCH}) \hat{\mathbf{x}} \tag{24}$$

where  $\hat{\mathbf{x}}(t)$  and  $\hat{\mathbf{x}}(t)$  represent the per unit value.

**Theorem.** *The system (24) is asymptotically stable, if and only if there exist matrices  $\mathbf{P}_1 = \mathbf{P}_1^T \geq 0$  and  $\mathbf{P}_2 = \mathbf{P}_2^T \geq 0$  satisfying the following conditions:*

$$\mathbf{P}_1 = c\mathbf{R}_1\mathbf{L} \tag{25}$$

$$\mathbf{A}^T\mathbf{P}_2 + \mathbf{P}_2\mathbf{A} + \mathbf{Q} - \mathbf{P}_2\mathbf{B}\mathbf{C}\mathbf{R}_2^{-1}\mathbf{C}^T\mathbf{B}^T\mathbf{P}_2 = 0 \tag{26}$$

$$c > \frac{\sigma_{\max}(\mathbf{R}_1\mathbf{L} \otimes (\mathbf{Q} - \mathbf{H}^T\mathbf{R}_2\mathbf{H}))}{\sigma_{>0\min}(\mathbf{L}^T\mathbf{R}_1\mathbf{L} \otimes \mathbf{H}^T\mathbf{R}_2\mathbf{H})} > 0 \tag{27}$$

where  $\mathbf{Q} = \mathbf{Q}^T \geq 0$ ,  $\mathbf{R}_1 = \mathbf{R}_1^T \geq 0$ ,  $\mathbf{R}_2 = \mathbf{R}_2^T \geq 0$ ,  $\sigma_{\max}(\mathbf{R}_1\mathbf{L}(\mathbf{Q} - \mathbf{H}^T\mathbf{R}_2\mathbf{H}))$  denotes the maximal singular values, and  $\sigma_{>0\min}(\mathbf{L}^T\mathbf{R}_1\mathbf{L}\mathbf{H}^T\mathbf{R}_2\mathbf{H})$  denotes the minimal nonzero singular value.

**Proof.** Define the feedback gain as:

$$\mathbf{H} = \mathbf{R}_2^{-1}\mathbf{C}^T\mathbf{B}^T\mathbf{P}_2 \tag{28}$$

Suppose  $\mathbf{Q}' = c^2(\mathbf{L}^T\mathbf{R}_1\mathbf{L}\mathbf{H}^T\mathbf{R}_2\mathbf{H}) - c(\mathbf{R}_1\mathbf{L}(\mathbf{A}^T\mathbf{P}_2 + \mathbf{P}_2\mathbf{A}))$ . From (27), we can obtain:

$$c^2\sigma_{>0\min}(\mathbf{L}^T\mathbf{R}_1\mathbf{L} \otimes \mathbf{H}^T\mathbf{R}_2\mathbf{H}) - c\sigma_{\max}(\mathbf{R}_1\mathbf{L} \otimes (\mathbf{Q} - \mathbf{H}^T\mathbf{R}_2\mathbf{H})) > 0 \Rightarrow \mathbf{Q}' \geq 0$$

The algebraic Riccati equation is  $(I_n A)^T P + P(I_n A) + Q - P(I_n BC)R^{-1}(I_n BC)^T P = 0$ , where  $P = P_1 P_2$ . Thus,  $Q'$  can be represented as:

$$\begin{aligned} Q' &= c^2(L^T R_1 L \otimes H^T R_2 H) - c(R_1 L \otimes (A^T P_2 + P_2 A)) \\ &= c^2(L^T R_1 L \otimes H^T R_2 H) + cR_1 L \otimes (Q - P_2 BCR_2^{-1} C^T B^T P_2) \\ &= P_1 R_1^{-1} P_1 \otimes P_2 BCR_2^{-1} C^T B^T P_2 + P_1 \otimes (Q - P_2 BCR_2^{-1} C^T B^T P_2) \end{aligned}$$

Define the Lyapunov function as  $V(x) = x^T P x$

$$\begin{aligned} \dot{V}(x) &= 2x^T P \dot{x} = 2x^T P(I_N \otimes A - cL \otimes BCH)x \\ &= 2x^T (P_1 \otimes P_2)(I_n \otimes A)x - 2cx^T (P_1 \otimes P_2)(L \otimes BCH)x \\ &= x^T (P_1 \otimes (A^T P_2 + P_2 A) - 2(P_1 R_1^{-1} P_1 \otimes P_2 BCR_2^{-1} C^T B^T P_2))x \\ &= x^T (P_1 \otimes (A^T P_2 + P_2 A) - 2(P(I_n \otimes BC) \otimes R^{-1}(I_n \otimes BC)^T P))x \\ &= x^T (P_1 \otimes (A^T P_2 + P_2 A) - 2(Q + P_1 \otimes (A^T P_2 + P_2 A)))x \\ &= -x^T (Q' + c^2(L \otimes H)^T (R_1 \otimes R_2)(L \otimes H))x \leq -x^T Q' x < 0 \end{aligned}$$

This completes the proof.

By choosing the coupling gain  $c$  and the feedback gain matrix  $H$  based on (27) and (28), the asymptotic stability of closed-loop system (24) can be ensured.

**Remark 2.** In this study, the design of consensus controller is based on the model in Figure 8. However, the design can also be extended to other models with different structures. For the consensus algorithm, the change of communication topology corresponds to the change of related elements in Laplace matrix, and the control effect will not be affected (the Lyapunov’s proof can also be applied). Hence, the designed controller is also applicable to different communication topologies of other MG structures.

### 5. Analysis of Circulating Current

In order to illustrate the effectiveness of the proposed method in reducing the circulating current between DG inverters, the relationship between circulating current and amplitude/angle of output voltage of DG inverter is analyzed. The simplified circuit schematic is shown in Figure 9.

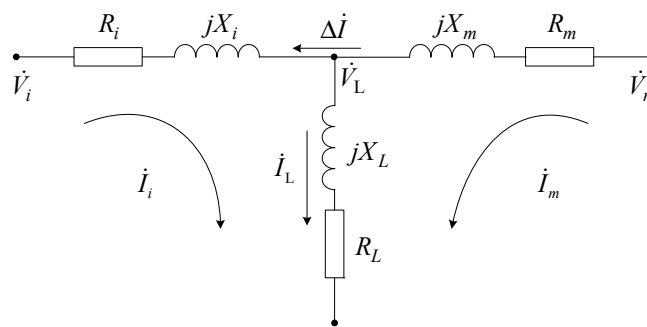


Figure 9. Simplified circuit schematic for two DG inverters.

From Figure 9, the relationship between the variables of two inverters is expressed as:

$$i_L = i_i + i_m \tag{29}$$

$$\dot{V}_L = Z_L(i_i + i_m) \tag{30}$$

$$i_i = (\dot{V}_i - \dot{V}_L)/Z_i \tag{31}$$

$$\dot{I}_m = (\dot{V}_m - \dot{V}_L) / Z_m \quad (32)$$

where  $Z_L = R_L + jX_L$ ,  $Z_i = R_i + jX_i$ ,  $Z_m = R_m + jX_m$ ,  $\dot{V}_L = E_L \angle \theta_L$ , and  $\dot{V}_m = E_m \angle \theta_m$ .

In (29), the load current is the vector sum of the two inverter currents. The load voltage related to the load current and load impedance can be expressed as:

$$\dot{V}_L = Z_L \left( \frac{\dot{V}_i - \dot{V}_L}{Z_i} + \frac{\dot{V}_m - \dot{V}_L}{Z_m} \right) = \frac{Z_i \dot{V}_m + Z_m \dot{V}_i}{Z_i + Z_m + Z_i Z_m / Z_L} \quad (33)$$

The circulating current is equal to the half of current difference between two inverters:

$$2\Delta\dot{I} = \dot{I}_i - \dot{I}_m = \frac{\dot{V}_i - \dot{V}_L}{Z_i} - \frac{\dot{V}_m - \dot{V}_L}{Z_m} \quad (34)$$

Inserting (33) into (34), the circulating current can be re-expressed as:

$$2\Delta\dot{I} = \frac{2(\dot{V}_i - \dot{V}_m) + (\dot{V}_i Z_m - \dot{V}_m Z_i) / Z_L}{Z_i + Z_m + Z_i Z_m / Z_L} \quad (35)$$

Assuming that the equivalent impedance of the bus is resistive, the impedance  $Z_L$  is replaced by  $R_L$ . Considering that the output impedance of inverter is mainly inductive ( $X_k \gg R_k$ ,  $k = i, m$ ), the circulating current is also derived as follows:

$$2\Delta\dot{I} = \frac{2(\dot{V}_i - \dot{V}_m) + j(\dot{V}_i X_m - \dot{V}_m X_i) / R_L}{j(X_i + X_m) - X_i X_m / R_L} \quad (36)$$

In order to analyze the active and reactive components of the circulating current separately, the formula (36) is written as:

$$2\Delta\dot{I} = I_a - jI_r \quad (37)$$

For the convenience of expression, define the following variables:

$$\begin{aligned} E'_i &= E_i X_m / R_L & E'_m &= E_m X_i / R_L \\ A &= (X_i + X_m)^2 + (X_i X_m / R_L)^2 \\ B &= (X_i X_m^2 + 2R_L^2 X_i + 2R_L^2 X_m) / R_L X_m \\ C &= (X_m X_i^2 + 2R_L^2 X_m + 2R_L^2 X_i) / R_L X_i \end{aligned}$$

Hence, the active and reactive components of the circulating current are written as:

$$\begin{aligned} I_a &= (E'_i((X_m - X_i) \cos \theta_i + B \sin \theta_i) - E'_m((X_i - X_m) \cos \theta_m + B \sin \theta_m)) / A \\ I_r &= (E'_i((X_i - X_m) \sin \theta_i + B \cos \theta_i) - E'_m((X_m - X_i) \sin \theta_m + B \cos \theta_m)) / A \end{aligned} \quad (38)$$

Assume  $X_i = X_m = X$ . Equation (38) can be rewritten as:

$$\begin{aligned} I_a &= (X^2 + 4R_L^2 / R_L)(E'_i \sin \theta_i - E'_m \sin \theta_m) / A \\ I_r &= (X^2 + 4R_L^2 / R_L)(E'_i \cos \theta_i - E'_m \cos \theta_m) / A \end{aligned} \quad (39)$$

Obviously, if the amplitude and angle of output voltage can be consistent, the active and reactive components of the circulating current become zero. Thus, the circulating current can be suppressed effectively by the proposed method.

## 6. Simulation Study

An islanded MG model with three parallel DGs is established. All DGs share the load power by the desired ratio of 2:3:4. The original load is 6 kW/3 kvar. The parameters for all the DGs are set as  $0.01 \Omega$ ,  $0.06 \text{ mH}$ ,  $1.5 \text{ mF}$ . The feeder impedance are set as  $0.612 + j3.18 \times 10^{-3} \Omega$ ,  $0.613 + j3.18 \times 10^{-3} \Omega$  and  $0.614 + j3.18 \times 10^{-3} \Omega$ , respectively. Other control parameters are set as  $c = 0.1$ ,  $m = 9.4 \times 10^{-5}$ , and  $n = 1.3 \times 10^{-3}$ .

### 6.1. Performance of Power Sharing

It is assumed that the MG operates in the islanding mode at  $t = 0 \text{ s}$ , and then operates stably. At  $t = 0.5 \text{ s}$ , the load with an extra 50% increase becomes 9 kW/4.5 kvar, and the coordinated control is applied. The corresponding performance of active power and reactive power is shown in Figure 10.

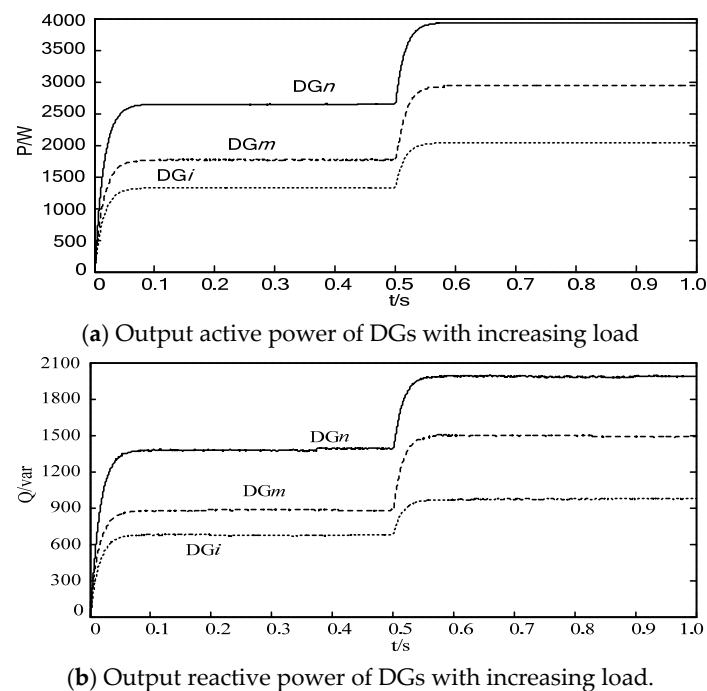


Figure 10. Experimental power waveforms under increasing load.

It can be known from the Figure 10a,b that the output active power and reactive power of DGs cannot be shared according to the desired ratio of 2:3:4 in the islanded mode during 0–0.5 s. This leads to that the output voltages of the DGs are not synchronous. However, the active power and reactive power of DGs are approximate to 2 kW/1 kvar, 3 kW/1.5 kvar, and 4 kW/2 kvar after  $t = 0.5 \text{ s}$ . It indicates that the power sharing is accurate in our method.

At  $t = 0.5 \text{ s}$ , the load with an extra 50% decrease becomes 3 kW/1.5 kvar, and the coordinated control is applied. The corresponding results are shown in Figure 11.

It can be seen from the Figure 11a,b that the output active power and reactive power of DGs cannot be shared according to the desired ratio without the coordinated control before  $t = 0.5 \text{ s}$ . When the coordinated control is used, the active power and reactive power of DGs are approximated to 0.67 kW/0.33 kvar, 1.00 kW/0.50 kvar, and 1.33 kW/0.67 kvar after  $t = 0.5 \text{ s}$ , which indicate that the active reactive powers can be shared more reasonably.

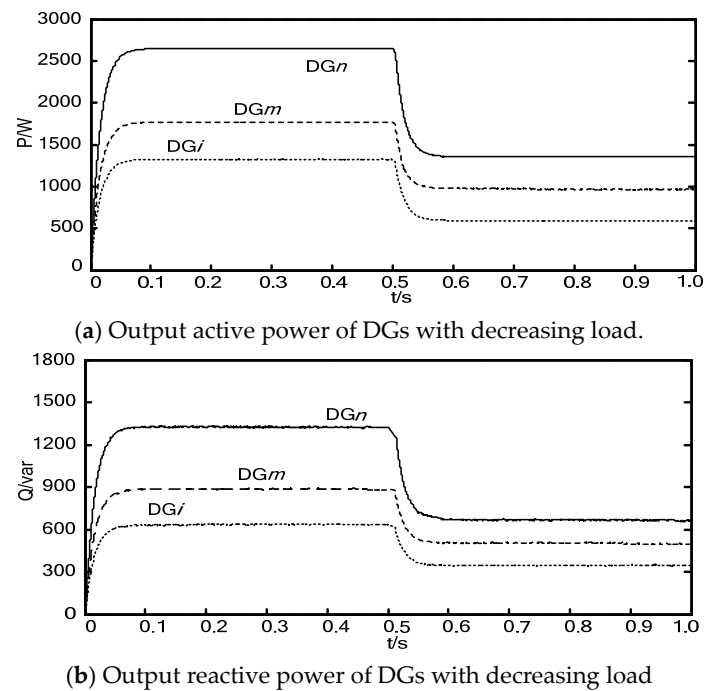


Figure 11. Experimental power waveforms with decreasing load.

### 6.2. Performance of Voltage Regulation

With the same MG model including three DGs in parallel, we have simulated the effect of DGs' voltage regulation of the coordinated controller. The specific experimental process is described as follows: (1) The bus voltage of the MG is set as 311 V, and each DG is only regulated by droop control; (2) 50% load increase and decrease are considered at  $t = 0.5$  s, respectively, and all DGs are regulated by coordinated control. The corresponding results are shown in Figure 12.

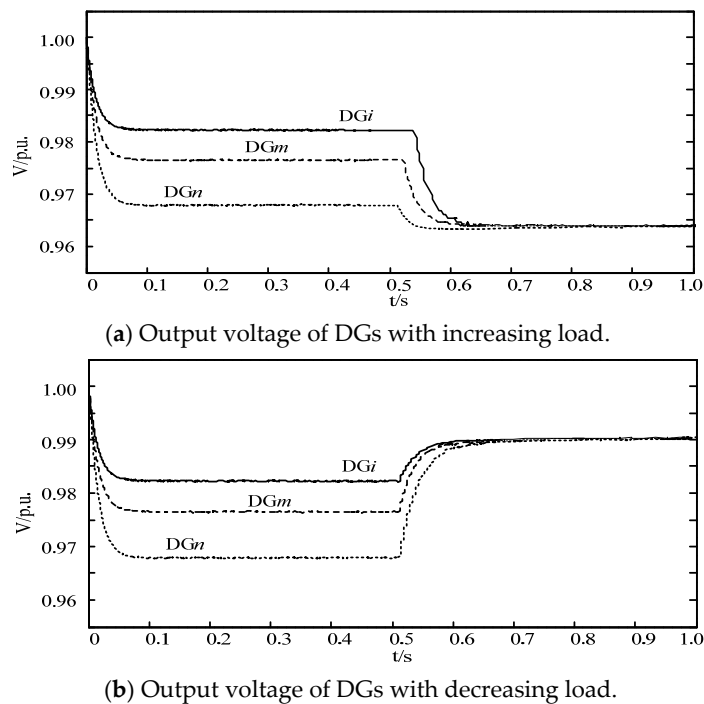
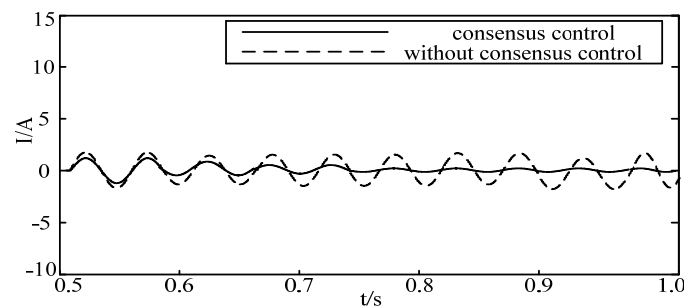


Figure 12. Experimental voltage waveforms with increasing/decreasing load.

As shown in Figure 12, the output voltages of the three DGs are respectively 0.985 p.u., 0.977 p.u., and 0.968 p.u. during 0–0.5 s. It is obvious that the output voltages of DGs are different because of the regulation error of decentralized droop control. When the coordinated control is used at  $t = 0.5$  s, the output voltages of all DGs become consistent after a 0.15 s transient process. For the two cases, the voltage of each DG will be respectively adjusted to 0.964 p.u. and 0.991 p.u. after  $t = 0.65$  s.

### 6.3. Performance of Circulating Current

In this case, the 50% load decreases at  $t = 0.5$  s, and all DGs are regulated by consensus control at the same time. As a contrast, we also carried out the experiment without consensus control after  $t = 0.5$  s. The corresponding performances of circulating current among DGs are shown in Figure 13.



**Figure 13.** Experimental circulating current waveforms.

It is found from the Figure 13 that the circulating current can be suppressed effectively when the consensus control is used at  $t = 0.5$  s. After about  $t = 0.9$  s (the consumed time for consensus control is almost 0.4 s), the circulating current is suppressed to 0. By contrast, the circulating current always exists if DGs are only controlled by droop control without consensus control.

### 6.4. Performance of Voltage Tracking

With the same MG model, 50% load is added at  $t = 0.5$  s in this case. To highlight the voltage tracking performance of FOPID control, the voltage at  $DG_i$  is selected as an example. PID controller and FOPID controller are simulated respectively. The specific results are shown in Figure 14.

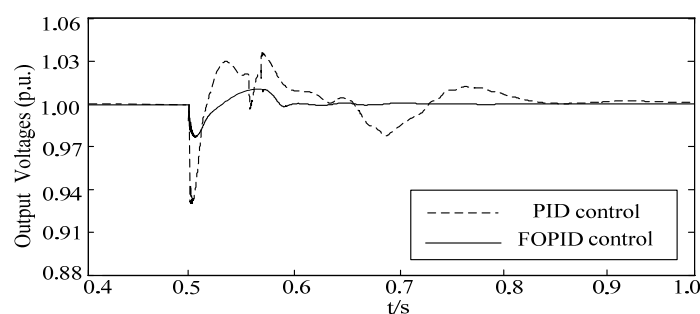


**Figure 14.** Experimental voltage waveforms of PID/FOPID control for  $DG_i$ .

It is shown in Figure 14 that before  $t = 0.5$  s, the output voltages of PID controller and FOPID controller are 1 p.u. After  $t = 0.5$  s, the output voltage of two controllers decreases because of the increasing load. It can be found that compared with the 0.07 p.u. overshoot and the 0.35 s restoring time of PID controller, they are smaller for the FOPID controller (0.025 p.u., 0.15 s). It implies that the FOPID controllers can improve the voltage tracking performance of DG.

## 7. Conclusions

In this paper, the decentralized coordinated control based on MAS has been proposed to improve power sharing, current quality, and voltage stability in a MG. By constructing the structure of MG based on MAS, the decentralized control and coordinated control have been implemented by the lower-level agent and the upper-level agent, respectively. Different from the conventional PID controller, the FOPID has been used for a better voltage tracking stability in the inner-loop controller of decentralized control. To reduce the DGs' voltage difference along with suppressing the circulating current, the multi-agent consensus algorithm has been used in coordinated control to synchronize the output voltages and currents of neighboring DGs. By the means of simulation, the accurate power sharing, small circulating current, stable voltage regulation have been achieved by our method. Besides, since neighboring DGs are considered in the dynamic equation design of coordinated control, our method can also achieve good voltage regulation stability in terms of a bigger MG with more DG access. The next work will focus on the further improvement of coordinated control by considering common communication constraints such as delay, packet-dropout, and topology change. The extension of our method in the MAS-based electricity market research will be also included.

**Author Contributions:** This paper is a collaborative effort of S.X., H.S., Z.Z., Q.G., B.Z., J.B. and B.Z.. S.X., H.S., Z.Z., Q.G., B.Z., J.B. and B.Z. conceived the methodology, conducted the experiments, and wrote the paper. All authors have read and agreed to the published version of the manuscript.

**Acknowledgments:** This research was funded by the National Natural Science Foundation of China under Grants 51977197, U1766202 and 51777195, Fundamental and Forecast Projects of State Grid Corporation of China "Theory Research on Response Driven Comprehensive Defense Control of Power System" under Grant XT71-18-014, Young Elite Scientists Sponsorship Program by CAST under Grant YESS20160157, and Young Elite Scientists Sponsorship Program by CSEE under Grant JLB-2017-305. And the APC was funded by all of them.

**Conflicts of Interest:** The authors declare no conflict of interest.

## Abbreviations

DG	Distributed generation
FC	Fuel cell
PID	Proportion-integration-differentiation
FOPID	Fractional order PID
MAS	Multi-agent system
MT	Micro turbines
PCC	Point of common coupling
PSO	Particle swarm optimization
PV	Photovoltaic
P-f	Active power-frequency
Q-U	Reactive power-voltage amplitude
WT	Wind turbine
MG	Micro-grid

## References

1. Sechilariu, M.; Wang, B.; Locment, F. Building integrated photovoltaic system with energy storage and smart grid communication. *IEEE Trans. Ind. Electron.* **2013**, *60*, 1607–1618. [[CrossRef](#)]
2. Zhang, Z.; Dou, C.; Zhang, B.; Yue, W. Voltage Distributed cooperative control considering communication security in photovoltaic power system. *IEEE Trans. Syst. Man Cybern. Syst.* **2019**, *49*, 1592–1600. [[CrossRef](#)]
3. Katiraei, F.; Iravani, M.R. Power management strategies for a microgrid with multiple distributed generation units. *IEEE Trans. Power Syst.* **2006**, *21*, 1821–1831. [[CrossRef](#)]
4. Guerrero, J.M.; Vasquez, J.C.; Matas, J.; Castilla, M.; De Vicuna, L.G.D. Control strategy for flexible microgrid based on parallel line-interactive UPS systems. *IEEE Trans. Ind. Electron.* **2009**, *56*, 726–736. [[CrossRef](#)]
5. Zhang, Z.; Dou, C.; Yue, D.; Zhang, B.; Xu, S.; Hayat, T.; Alsaedi, A. An event-triggered secondary control strategy with network delay in islanded microgrids. *IEEE Syst. J.* **2019**, *13*, 1851–1860. [[CrossRef](#)]

6. Elrayyah, A.; Cingoz, F.; Sozer, Y. Construction of nonlinear droop relations to optimize islanded microgrid operation. *IEEE Trans. Ind. Appl.* **2015**, *51*, 3404–3413. [[CrossRef](#)]
7. Zhang, Z.; Dou, C.; Yue, D.; Zhang, B.; Luo, W. A decentralized islanded microgrids control method for frequency restoration and accurate reactive power sharing. *J. Frankl. Inst.* **2018**, *355*, 8874–8890. [[CrossRef](#)]
8. He, J.; Pan, Y.; Liang, B.; Wang, C. A simple decentralized islanding microgrid power sharing method without using droop control. *IEEE Trans. Smart Grid* **2018**, *9*, 6128–6239. [[CrossRef](#)]
9. Zhou, J.; Zhang, H.; Sun, Q.; Ma, D.; Huang, B. Event-based distributed active power sharing control for interconnected AC and DC microgrids. *IEEE Trans. Smart Grid* **2018**, *9*, 6815–6828. [[CrossRef](#)]
10. Shafiee, Q.; Nasirian, V.; Vasquez, J.C.; Guerrero, J.M.; Davoudi, A. A multi-functional fully distributed control framework for AC microgrids. *IEEE Trans. Smart Grid* **2018**, *9*, 3247–3258. [[CrossRef](#)]
11. Zhang, Z.; Dou, C.; Yue, D.; Zhang, B.; Zhang, T. Photovoltaic voltage regulation through distributed power compensation considering communication delay. *Adv. Theory Simul.* **2020**, *3*. [[CrossRef](#)]
12. Wang, P.; Lu, X.; Yang, X.; Wang, W.; Xu, D. An improved distributed secondary control method for DC microgrids with enhanced dynamic current sharing performance. *IEEE Trans. Power Electron.* **2016**, *31*, 6658–6673. [[CrossRef](#)]
13. Zhang, B.; Dou, C.; Yue, D.; Zhang, Z.; Zhang, T. A packet loss-dependent event-triggered cyber-physical cooperative control strategy for islanded microgrid. *IEEE Trans. Cybern.* **2019**. [[CrossRef](#)] [[PubMed](#)]
14. Zhang, B.; Dou, C.X.; Yue, D.; Zhang, Z.; Zhang, T. A cyber-physical cooperative hierarchical control strategy for islanded microgrid facing with random communication failure. *IEEE Syst. J.* **2020**. [[CrossRef](#)]
15. Mao, M.; Jin, P.; Hatziargyriou, N.D.; Chang, L. Multiagent-based hybrid energy management system for microgrids. *IEEE Trans. Sustain. Energy* **2014**, *5*, 938–946. [[CrossRef](#)]
16. Dou, C.; Hao, D.; Jin, B.; Wang, W.; An, N. Multi-agent-system-based decentralized coordinated control for large power systems. *Int. J. Electr. Power Energy Syst.* **2014**, *58*, 130–139. [[CrossRef](#)]
17. Liu, W.; Gu, W.; Sheng, W.; Meng, X.; Wu, Z.; Chen, W. Decentralized multi-agent system-based cooperative frequency control for autonomous microgrids with communication constraints. *IEEE Trans. Sustain. Energy* **2014**, *5*, 446–456. [[CrossRef](#)]
18. Sun, Q.; Han, R.; Zhang, H.; Zhou, J.; Guerrero, J.M. A multiagent-based consensus algorithm for distributed coordinated control of distributed generators in the energy internet. *IEEE Trans. Smart Grid* **2015**, *6*, 3006–3019. [[CrossRef](#)]
19. Ren, W.; Beard, R.W. Consensus seeking in multiagent systems under dynamically changing interaction topologies. *IEEE Trans. Autom. Control* **2005**, *50*, 655–661. [[CrossRef](#)]
20. Olfati-Saber, R.; Fax, J.A.; Murray, R.M. Consensus and cooperation in networked multi-agent systems. *Proc. IEEE* **2007**, *95*, 215–233. [[CrossRef](#)]
21. Li, Z.; Duan, Z.; Chen, G.; Huang, L. Consensus of multiagent systems and synchronization of complex networks: A unified viewpoint. *IEEE Trans. Circuits Syst. I Regul. Pap.* **2010**, *57*, 213–224.
22. Fax, J.A.; Murray, R.M. Information flow and cooperative control of vehicle formations. *IEEE Trans. Autom. Control* **2004**, *49*, 1465–1476. [[CrossRef](#)]
23. He, J.; Li, Y.; Guerrero, J.M.; Blaabjerg, F.; Vasquez, J.C. An islanding microgrid power sharing approach using enhanced virtual impedance control scheme. *IEEE Trans. Power Electron.* **2013**, *28*, 5272–5282. [[CrossRef](#)]
24. Zhong, Q. Robust droop controller for accurate proportional load sharing among inverters operated in parallel. *IEEE Trans. Ind. Electron.* **2013**, *60*, 1281–1290. [[CrossRef](#)]
25. Pogaku, N.; Prodanović, M.; Green, T.C. Modeling, analysis and testing of autonomous operation of an inverter-based microgrid. *IEEE Trans. Power Electron.* **2014**, *22*, 613–625. [[CrossRef](#)]
26. Zhang, Z.; Dou, C.; Yue, D.; Zhang, B.; Li, F. Neighbor-prediction-based networked hierarchical control for islanded microgrid. *Int. J. Electr. Power Energy Syst.* **2019**, *104*, 734–743. [[CrossRef](#)]
27. Majumder, R.; Chaudhuri, B.; Ghosh, A.; Majumder, R.; Ledwich, G.; Zare, F. Improvement of stability and load sharing in an autonomous microgrid using supplementary droop control loop. *IEEE Trans. Power Syst.* **2012**, *25*, 796–808. [[CrossRef](#)]
28. Dou, C.; Zhang, Z.; Yue, D.; Song, M. Improved droop control based on virtual impedance and virtual power source in low-voltage microgrid. *IET Gener. Transm. Distrib.* **2017**, *11*, 1046–1054. [[CrossRef](#)]
29. Monje, C.A.; Vinagre, B.M.; Feliu, V.; Chen, Y. Tuning and auto-tuning of fractional order controllers for industry applications. *Control Eng. Pract.* **2008**, *16*, 798–812. [[CrossRef](#)]

30. Zamani, M.; Karimi-Ghartemani, M.; Sadati, N.; Parniani, M. Design of a fractional order PID controller for an AVR using particle swarm optimization. *Control Eng. Pract.* **2009**, *17*, 1380–1387. [[CrossRef](#)]
31. Cao, J.Y.; Cao, B.G. Design of fractional order controller based on particle swarm optimization. *Int. J. Control Autom. Syst.* **2006**, *4*, 775–781.
32. Chang, W.; Shih, S.P. PID controller design of nonlinear systems using an improved particle swarm optimization approach. *Commun. Nonlinear Sci. Numer. Simul.* **2010**, *11*, 3632–3639. [[CrossRef](#)]
33. Li, P.; Xu, D.; Zhou, Z. Stochastic optimal operation of microgrid based on chaotic binary particle swarm optimization. *IEEE Trans. Smart Grid* **2016**, *7*, 66–73. [[CrossRef](#)]
34. Zhang, H.; Lewis, F.L.; Das, A. Optimal design for synchronization of cooperative systems: State feedback, observer and output feedback. *IEEE Trans. Autom. Control* **2011**, *56*, 1948–1952. [[CrossRef](#)]
35. Bidram, A.; Lewis, F.L.; Davoudi, A. Distributed control systems for small-scale power networks: Using multiagent cooperative control theory. *IEEE Control Syst. Mag.* **2014**, *34*, 56–77.
36. Bidram, A.; Davoudi, A.; Lewis, F.L. Distributed cooperative secondary control of microgrids using feedback linearization. *IEEE Trans. Power Syst.* **2013**, *28*, 3462–3470. [[CrossRef](#)]
37. Movric, K.H.; Lewis, F.L. Cooperative optimal control for multi-agent systems on directed graph topologies. *IEEE Trans. Autom. Control* **2014**, *59*, 769–774. [[CrossRef](#)]



© 2020 by the authors. Licensee MDPI, Basel, Switzerland. This article is an open access article distributed under the terms and conditions of the Creative Commons Attribution (CC BY) license (<http://creativecommons.org/licenses/by/4.0/>).